Observation of Magnetic Helicoidal Dichroism with Extreme Ultraviolet Light Vortices

Mauro Fanciulli,[1,2,*,†] Matteo Pancaldi,[3,*] Emanuele Pedersoli,[3] Mekha Vimal,[1] David Bresteau,[1] Martin Luttmann,[1] Dario De Angelis,[3] Primož Rebernik Ribič,[3] Benedikt Rösner,[4] Christian David,[4] Carlo Spezzani,[3] Michele Manfredda,[3] Ricardo Sousa,[5] Ioan-Lucian Prejbeanu,[5] Laurent Vila,[5] Bernard Dieny,[5] Giovanni De Ninno,[3,6] Flavio Capotondi,[3] Maurizio Sacchi,[7,8] and Thierry Ruchon[1,‡]

[1]*Université Paris-Saclay, CEA, CNRS, LIDYL, 91191 Gif-sur-Yvette, France*
[2]*Laboratoire de Physique des Matériaux et Surfaces, CY Cergy Paris Université, 95031 Cergy-Pontoise, France*
[3]*Elettra-Sincrotrone Trieste S.C.p.A., 34149 Basovizza, Trieste, Italy*
[4]*Paul Scherrer Institut, 5232 Villigen-PSI, Switzerland*
[5]*Université Grenoble Alpes, CNRS, CEA, Grenoble INP, IRIG-SPINTEC, 38000 Grenoble, France*
[6]*Laboratory of Quantum Optics, University of Nova Gorica, 5001 Nova Gorica, Slovenia*
[7]*Sorbonne Université, CNRS, Institut des NanoSciences de Paris, INSP, 75005 Paris, France*
[8]*Synchrotron SOLEIL, L'Orme des Merisiers, Saint-Aubin, B. P. 48, 91192 Gif-sur-Yvette, France*

(Received 24 March 2021; accepted 19 January 2022; published 16 February 2022)

We report on the experimental evidence of magnetic helicoidal dichroism, observed in the interaction of an extreme ultraviolet vortex beam carrying orbital angular momentum with a magnetic vortex. Numerical simulations based on classical electromagnetic theory show that this dichroism is based on the interference of light modes with different orbital angular momenta, which are populated after the interaction between light and the magnetic topology. This observation gives insight into the interplay between orbital angular momentum and magnetism and sets the framework for the development of new analytical tools to investigate ultrafast magnetization dynamics.

DOI: 10.1103/PhysRevLett.128.077401

Beyond plane waves, light beams may feature helical wave fronts, with the Poynting vector precessing with time around the beam's propagation axis [1]. The number of intertwined helices spiraling clockwise or anticlockwise defines the topological charge $\ell \in \mathbb{Z}$, which is associated with the orbital angular momentum (OAM) of the light vortices. This is independent from light's polarization state, which instead is associated with a spin angular momentum (SAM) [2]. OAM light beams are nowadays harnessed for an ever increasing scope of applications covering different fields, from microscopy [3–5] and biology [6,7] to telecommunications [8,9] and quantum technologies [10,11]. Vortex beams also play a role in spectroscopy, where the coupling between the OAM and the internal degrees of freedom of atoms, atomic ions, or molecules has been exploited to transfer OAM to these species [12–15] and to enhance enantiomeric sensitivity [16,17]. Also, a rich variety arises for the investigation and manipulation of topologically complex objects, such as chiral magnetic structures [18] and skyrmions [19–21]. In the same way as tuning the wavelength is used to achieve chemical contrast, or tuning the polarization to achieve magnetic contrast, controlling the OAM state of a vortex beam has the potential to provide topological contrast in systems possessing a well-defined handedness. This general statement can eventually find applications in many different extreme ultraviolet (XUV) and x-ray based techniques, like elastic or inelastic scattering and photoelectron emission. The study of magnetic structures is a particularly appealing case, for their practical importance and for the possible control of their topology.

Over the last decade, the development of highly coherent sources and tailored optical schemes has opened new possibilities for generating structured light vortices in the XUV [22–29] and x-ray [30–35] regimes, paving the way to their spectroscopic applications. In this context, magnetic helicoidal dichroism (MHD) has been recently predicted [36], in analogy to the SAM-dependent magnetic circular dichroism (MCD). Upon interaction (reflection or transmission) of a pure Laguerre-Gaussian mode of topological charge ℓ with a magnetic surface, MHD consists in an intensity redistribution into all modes $\ell + n$ in the outgoing beam, where n represents all the azimuthal decomposition coefficients of the magnetic structure symmetry [36]. Different from MCD, MHD is sensitive to the overall topology of the spin texture, it vanishes for homogeneous structures, and is not self-similar if one inverts either the topological charge of the beam or the magnetization direction.

Among a great variety of magnetic structures in two [37] or three dimensions [38], magnetic vortices (MVs) are particularly promising for technological applications [39,40]. They can form in mesoscopic dots that are much larger than their thickness [41], leading to a planar

magnetization with curling direction either clockwise ($m = +1$) or anticlockwise ($m = -1$), which we can associate with a toroidal moment [42,43]. They have been shown to be particularly robust against perturbations [44] and present a rich subnanosecond dynamics [45]. Because of their symmetry, MVs are also a particularly simple test case for MHD, since they only present $n = \pm 1$ [36].

In this Letter, we report on the experimental observation of MHD by measuring the resonant scattering of XUV radiation carrying OAM from a permalloy (Py, $Fe_{20}Ni_{80}$) dot in MV micromagnetic configuration. We compare the experimental results to theoretical predictions [36] and we interpret them in terms of the interference between the different $\ell + n$ modes of the reflected light. Our study illustrates the potential of MHD as a new optical tool for the investigation of magnetic structures and their topology.

The experiment was performed at the DiProI beam line [46] of the FERMI free-electron laser (FEL) [47] using the setup sketched in Fig. 1(a). The spatially coherent close-to-Gaussian FEL beam is focused on the sample by one of three available silicon zone plates [48] mounted on a movable stage. One is a Fresnel zone plate producing a focused beam with $\ell = 0$; the other two are spiraling zone plates (SZPs) that impart OAM to the beam with either $\ell = -1$ or $\ell = +1$. The properties of the zone plates are detailed in [26]. An electron microscope image of the SZP

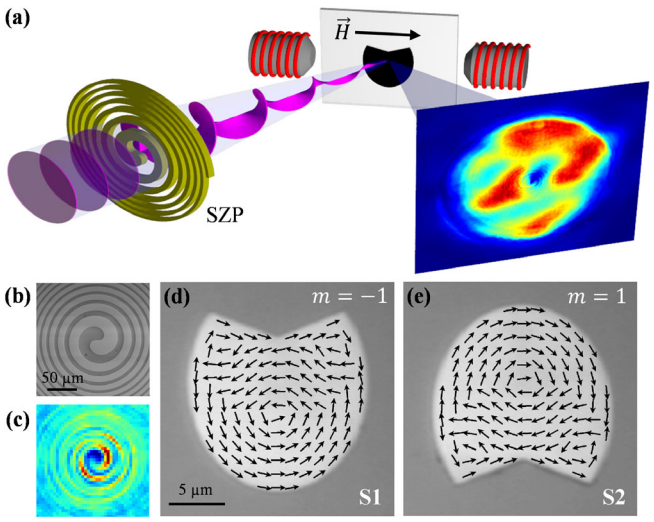

FIG. 1. (a) Schematics of the experimental setup at the DiProI beam line, showing the incoming FEL beam with planar wave front, a SZP that imparts OAM to the FEL beam, the sample placed between the poles of the electromagnet and the image of the scattered beam. (b) Scanning electron microscope image of one SZP ($\ell = +1$). (c) Far field image of the interference pattern of the corresponding OAM beam and the undiffracted, OAM-free beam, featuring a spiraling intensity pattern. (d),(e) Magnetic dots $S1$ and $S2$ with corresponding remanent magnetization after applying a pulse of saturating external field $\vec{H}$ as in (a). An opposite field reverses the curling direction m of the remanent magnetization in both samples.

for $\ell = +1$ is shown in Fig. 1(b), while in Fig. 1(c) the direct image of the beam with OAM collected by a CCD camera shows the expected spiral-shaped far field interference pattern with the undiffracted beam [26,49].

The photon energy was set to 52.8 eV in order to match the Fe $3p \rightarrow 3d$ core resonance [50]. This approach, which is standard in x-ray dichroism, allows one to simultaneously enhance the magneto-optical effects (that would be otherwise negligible at XUV wavelengths, compared to charge scattering) and to introduce element selectivity. The linearly p-polarized XUV beam impinged on the center of the sample at an angle of 48° from the normal, i.e., close to the Brewster extinction condition, in order to maximize the magnetic signal. Using a knife edge scan, we measured a spot size of about 4 μm (full width at half maximum) at the sample plane, in agreement with previous characterizations [51]. The reflected beam is collected by a CCD camera placed 150 mm from the sample.

The samples [$S1$ and $S2$, Figs. 1(d) and 1(e)] are two identical and π-rotated ellipsoidal Py dots with a triangular indent, prepared on the same Si substrate. They are 80 nm thick, their short diameter is 15 μm, and they are protected by a ≈3 nm Al layer (oxidized in air) (see Supplemental Material [48]). Their exact shape was optimized by micromagnetic calculations [52] in order to satisfy two criteria: (i) feature at remanence a single stable MV with a diameter larger than the XUV beam spot size; (ii) enable the switching of the remanent vortex curling direction m by *in situ* application of a moderate external magnetic field pulse. The calculated remanent magnetization after a +20 mT in-plane magnetic pulse [arrow in Fig. 1(a)] shows that MVs with $m = -1$ and $m = +1$ are formed in $S1$ and $S2$ [Figs. 1(d) and 1(e)], respectively, providing a simple way of cross-checking our experimental results. Reversing the magnetic pulse direction switches the sign of m in both MVs. Further experimental details are given in the Supplemental Material [48].

For each sample, we evaluate the dichroic signal by switching the sign of the external magnetic field pulse before measuring at remanence, so that no mechanical or optical adjustment of the setup is required, guaranteeing optimal stability in the measurement conditions. Also, in this way, nonmagnetic contributions to the scattered intensity are largely suppressed from the difference signal. Figures 2(a)–2(f) show the experimental dichroism on the intensity profile of the reflected beam for three incoming ℓ values and for the two samples. Details of the data analysis are given in the Supplemental Material [48]. For sample $S1$, we observe a left-right asymmetry for $\ell = 0$ [Fig. 2(c)] and opposite spiral asymmetries for opposite topological charges of the OAM beam $\ell = \pm 1$ [Figs. 2(a) and 2(e)], showing the differential dependence on the topological charge of the OAM beam. The measured MHD signal is on the order of 20%. The result is reproduced in $S2$ [Figs. 2(b), 2(d), and 2(f)], where the

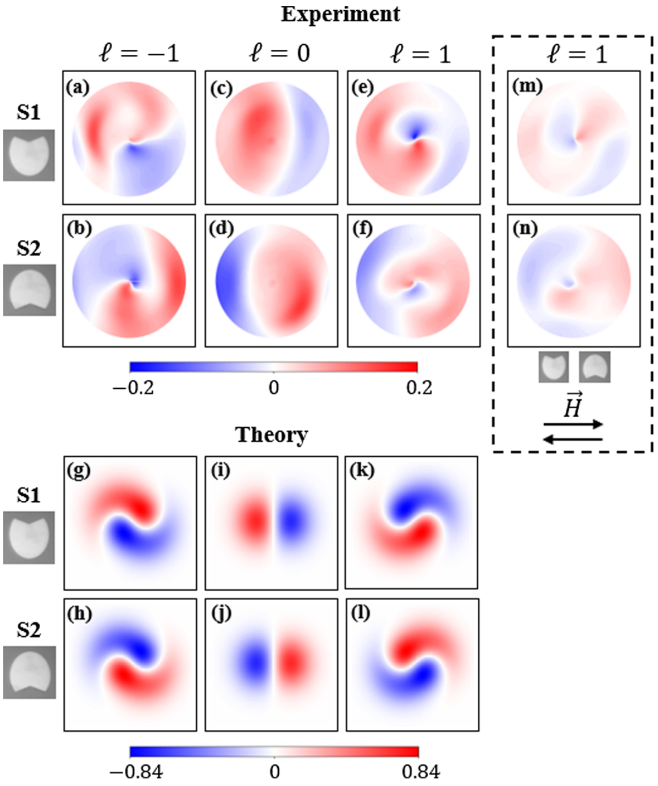

FIG. 2. (a)–(f) Experimental dichroism (corresponding to MHDm) for $\ell = -1, 0, +1$ for MVs in dot $S1$ (top) and $S2$ (bottom). (g)–(l) Numerical simulations for the same experimental parameters. (m),(n) Same as (e),(f), with the same color scale, but with a constant magnetic field applied during the acquisition in order to homogenize sample's magnetization; to be used as a reference. The images corresponding to (a)–(d) can be found in the Supplemental Material [48].

color pattern is reversed since the two samples always have opposite m. This demonstrates the magnetic nature of the observed dichroic signal rather than possible asymmetries induced by the experimental setup. It is worth noting that the symmetry relations observed in Figs. 2(a)–2(f) are almost canceled when the MV topology is perturbed by applying an external magnetic field (Figs. 2(m) and 2(n) and Supplemental Material [48]). The azimuthal Fourier component with period 2π [48], which generates a signal of $\pm 20\%$ in presence of the MV, is strongly reduced (down to ca. $\pm 5\%$ amplitude) when an external magnetic field erases the vortex structure.

In order to interpret the experimental results, we implemented a numerical model for MHD based on Ref. [36], with a perfect Gaussian beam as input, ideal optics, and perfect centering of the beam on the MV. The results of the simulations for the same scattering geometry as in the experiment are shown in Figs. 2(g)–2(l). They can be directly compared with Figs. 2(a)–2(f), showing a good agreement for all configurations. Quantitatively, the experimental dichroism is lower than expected. We believe this is mainly due to the nonmagnetic signal coming from the oxidized Al-capping layer not taken into account in the simulations [48]. The imperfect symmetry of the experimental images [evident, e.g., in Figs. 2(c) and 2(d)] is due to the approximate alignment of the OAM beam on the vortex core, which is impossible to visualize *in situ* (see Supplemental Material [48] for more details). Here it is important to stress that the dependence of the MHD signal on the topological charge is not linked to the particular chosen reflection geometry close to the Brewster angle. From further simulations [48] we predict that, even close to normal incidence, the asymmetry for $\ell = 0$ (left-right) is different from $\ell = \pm 1$ (top-bottom), while the spiral asymmetry of Fig. 2 is due to a combination with geometric effects [36].

In general, in order to evaluate the MHD, three relevant combinations of differences between signals obtained with given values of topological charge of the beam and the curling direction of the MV can be considered [48]. Defining $I_{\ell,m}$ the far field intensity of the reflected beam, we classify these three kinds of dichroisms as [36]

$$\mathrm{MHD}\ell = (I_{\ell,m} - I_{-\ell,m})/(I_{\ell,m} + I_{-\ell,m}) \tag{1a}$$

$$\mathrm{MHD}m = (I_{\ell,m} - I_{\ell,-m})/(I_{\ell,m} + I_{\ell,-m}) \tag{1b}$$

$$\mathrm{MHD}\ell m = (I_{\ell,m} - I_{-\ell,-m})/(I_{\ell,m} + I_{-\ell,-m}). \tag{1c}$$

The dichroism presented in Fig. 2 corresponds to MHDm, since switching the magnetic field direction corresponds to switching the sign of m in the MV for a fixed value of ℓ. In Fig. 3, the other two kinds of MHD from simulations are shown. The dichroic intensity map of MHDm [Figs. 2(g) and 2(k)] differs from MHDℓ [Figs. 3(a) and 3(b)], which ensures a nonzero MHDℓm [Figs. 3(c) and 3(d)]. This is a crucial difference with respect to MCD, where switching the sample magnetization or the light polarization leads to equivalent results. From the experimental point of view, changing m is obtained simply by a magnetic field pulse. On the contrary, changing ℓ implies replacing the SZP, affecting the photon beam trajectory and amplifying the issues in photon–vortex-core alignment already mentioned above. This makes our experimental observation less reliable for MHDℓ and MHDℓm than for MHDm [48].

In order to complement the theoretical analysis proposed in [36], it is interesting to look into the physical mechanism at the origin of MHDm. The local values of the magneto-optical constants are proportional to the curling magnetization, and the reflectivity matrix will thus depend on the azimuth ϕ. This can be used to intuitively retrieve the simple selection rule $\Delta\ell = \pm 1$ for reflection by a MV [36]. In fact, the magnetization terms of the MV, and hence the reflectivity coefficients, vary as $\cos(\phi)$ up to a constant phase term, while the azimuthal dependence of the incoming electric field due to the OAM is $\cos[-(2\pi/\lambda)z - \ell\phi]$, with λ and z being the light wavelength and the propagation

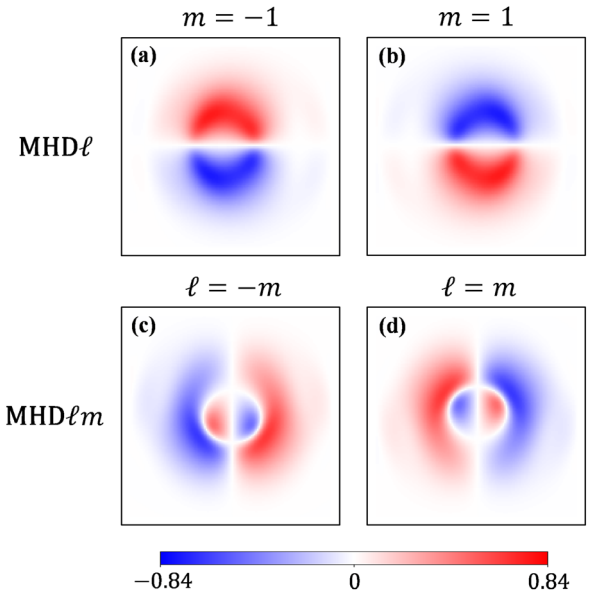

FIG. 3. Numerical simulations with same experimental parameters of (a),(b) MHDℓ for different m and (c),(d) MHDℓm for different combinations of ℓ and m.

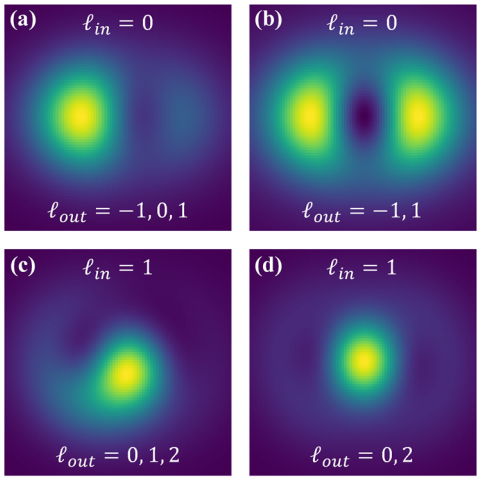

FIG. 4. (a) Far field intensity of a beam with $\ell_{\mathrm{in}} = 0$ reflected by a MV with $m = +1$. (b) Same as (a) when the outgoing mode $\ell_{\mathrm{out}} = \ell_{\mathrm{in}}$ is suppressed. (c),(d) The same results as (a) and (b) when $\ell_{\mathrm{in}} = 1$.

direction, respectively. Without considering geometric effects [36], the magnetic contribution to the outgoing electric field is given by the product of those two terms and will thus show $(\ell \pm 1)\phi$ components, and only these, while the nonmagnetic one is only given by a reflection of the ℓ mode. The propagation of the ℓ and $\ell \pm 1$ modes to the far field will result in interferences in the intensity profile, which is what causes the asymmetries of MHD. Note that this is valid for every incoming ℓ, including $\ell = 0$.

To be more specific, let us consider a p-polarized beam with $\ell_{\mathrm{in}} = 0$, which is a standard Gaussian plane wave without OAM. Figure 4(a) shows the far field simulated intensity after reflection from a $m = +1$ MV, featuring a left-right imbalance that reverses for the case $m = -1$ [48], leading to MHDm [Fig. 2(i)]. If we suppress the propagation of the outgoing mode $\ell_{\mathrm{out}} = 0$ in the simulation and leave only $\ell_{\mathrm{out}} = \pm 1$, we obtain the intensity in Fig. 4(b). This is the typical shape of a Hermite-Gaussian beam of index 1. We can draw two important conclusions. One is that even a standard Gaussian beam with $\ell = 0$ reflected by a magnetic structure such as a MV contains equal weights of modes with opposite nonzero OAM. This is a largely overlooked observation that can be used as a fresh way to look at magneto-optical scattering phenomena. The second conclusion is that the dichroic signal in MHD originates from the interference of the main incoming mode $\ell_{\mathrm{out}} = \ell_{\mathrm{in}}$ with the newly generated ones. This can also be seen, for example, for the case of $\ell_{\mathrm{in}} = 1$. In Fig. 4(d), where $\ell_{\mathrm{out}} = 1$ is suppressed from the reflected beam, one finds signatures of a second-order Hermite-Gaussian beam, while the full beam of Fig. 4(c) is the result of the interference with the central mode, including the $\ell = 1$ mode. In this case, a spiraling shape is obtained. Its mirrored image on the horizontal axis is obtained when one considers $\ell_{\mathrm{in}} = -1$ instead, mirrored on the vertical axis when $\ell_{\mathrm{in}} = -1$ and $m = -1$ and mirrored on both axis when $\ell_{\mathrm{in}} = +1$ and $m = -1$ [48]. The fact that these four cases are not equivalent explains why MHDm and MHDℓ are different, and thus the existence of MHDℓm.

In conclusion, we presented the experimental evidence of magnetic helicoidal dichroism in the resonant reflection of an XUV beam that carries OAM by a magnetic vortex and found a good agreement with theoretical predictions. In particular, we identify the specific dependence of MHD on the sign of the optical (ℓ) and magnetic (m) vortices. Other configurations of OAM and light polarization could be explored [48], providing altogether a new way to look at the magneto-optical scattering process in terms of OAM, as discussed also for the case of an $\ell = 0$ incoming beam.

It is straightforward to extend this approach to other complex magnetic structures. For example, in analogy with the recent observation that infrared vortex beams with opposite ℓ are sensitive to dipolar chiral nanohelix [53,54], one can envision to use MHD for XUV and soft x-ray beams with OAM in order to detect the helical direction of complex 3D spiral spin structures [55] or to study chiral domain walls and skyrmions in magnetic films with strong Dzyaloshinskii-Moriya interaction [56]. Conversely, different structures can be engineered in order to tailor or analyze the OAM content of a light beam [33,35]. A limit of our interpretation is that it is based on classical electromagnetism. A microscopic theory has still to be developed and questions about a possible local exchange of OAM between light and matter remain open. Finally, the feasibility of this experiment with a FEL source naturally opens up the study of MHD in the time domain, as recently performed in nanoplasmonics [57,58]. MHD could then become a

powerful experimental tool for the study of the ultrafast dynamics of magnetic materials and of their topological properties [59,60], but also a way to control and manipulate them, in a similar fashion as in the inverse Faraday effect with SAM [61].

This work was supported by the Agence Nationale pour la Recherche (under Contracts No. ANR11-EQPX0005-ATTOLAB, No. ANR14-CE320010-Xstase and Investissement d'avenir Labex Palm Grant No. ANR-10-LABX-0039-PALM), the Swiss National Science Foundation project No. P2ELP2_181877, the Plateforme Technologique Amont de Grenoble, with the financial support of the CNRS Renatech network, and the EU-H2020 Research and Innovation Programme, No. 654360 NFFA-Europe.

*These authors contributed equally to this work.
†mauro.fanciulli@u-cergy.fr
‡thierry.ruchon@cea.fr

[1] L. Allen, M. W. Beijersbergen, R. J. C. Spreeuw, and J. P. Woerdman, Orbital angular momentum of light and the transformation of Laguerre-Gaussian laser modes, Phys. Rev. A **45**, 8185 (1992).
[2] K. Y. Bliokh and F. Nori, Transverse and longitudinal angular momenta of light, Phys. Rep. **592**, 1 (2015).
[3] T. A. Klar and S. W. Hell, Subdiffraction resolution in far-field fluorescence microscopy, Opt. Lett. **24**, 954 (1999).
[4] S. Wei, T. Lei, L. Du, C. Zhang, H. Chen, Y. Yang, S. W. Zhu, and X.-C. Yuan, Sub-100 nm resolution PSIM by utilizing modified optical vortices with fractional topological charges for precise phase shifting, Opt. Express **23**, 30143 (2015).
[5] F. Tamburini, G. Anzolin, G. Umbriaco, A. Bianchini, and C. Barbieri, Overcoming the Rayleigh Criterion Limit with Optical Vortices, Phys. Rev. Lett. **97**, 163903 (2006).
[6] L. Paterson, M. P. MacDonald, J. Arlt, W. Sibbett, P. E. Bryant, and K. Dholakia, Controlled rotation of optically trapped microscopic particles, Science **292**, 912 (2001).
[7] D. G. Grier, A revolution in optical manipulation, Nature (London) **424**, 810 (2003).
[8] R. Fickler, G. Campbell, B. Buchler, P. K. Lam, and A. Zeilinger, Quantum entanglement of angular momentum states with quantum numbers up to 10,010, Proc. Natl. Acad. Sci. U.S.A. **113**, 13642 (2016).
[9] L. Gong, Q. Zhao, H. Zhang, X.-Y. Hu, K. Huang, J.-M. Yang, and Y.-M. Li, Optical orbital-angular-momentum-multiplexed data transmission under high scattering, Light **8**, 27 (2019).
[10] A. M. Yao and M. J. Padgett, Orbital angular momentum: Origins, behavior and applications, Adv. Opt. Photonics **3**, 161 (2011).
[11] Y. Shen, X. Wang, Z. Xie, C. Min, X. Fu, Q. Liu, M. Gong, and X. Yuan, Optical vortices 30 years on: OAM manipulation from topological charge to multiple singularities, Light **8**, 90 (2019).
[12] K. A. Forbes and D. L. Andrews, Optical orbital angular momentum: Twisted light and chirality, Opt. Lett. **43**, 435 (2018).
[13] C. T. Schmiegelow, J. Schulz, H. Kaufmann, T. Ruster, U. G. Poschinger, and F. Schmidt-Kaler, Transfer of optical orbital angular momentum to a bound electron, Nat. Commun. **7**, 12998 (2016).
[14] A. Afanasev, C. E. Carlson, C. T. Schmiegelow, J. Schulz, F. Schmidt-Kaler, and M. Solyanik, Experimental verification of position-dependent angular-momentum selection rules for absorption of twisted light by a bound electron, New J. Phys. **20**, 023032 (2018).
[15] G. De Ninno *et al.*, Photoelectric effect with a twist, Nat. Photonics **14**, 554 (2020).
[16] W. Brullot, M. K. Vanbel, T. Swusten, and T. Verbiest, Resolving enantiomers using the optical angular momentum of twisted light, Sci. Adv. **2**, e1501349 (2016).
[17] J. Ni, S. Liu, D. Wu, Z. Lao, Z. Wang, K. Huang, S. Ji, J. Li, Z. Huang, Q. Xiong, Y. Hu, J. Chu, and C.-W. Qiu, Gigantic vortical differential scattering as a monochromatic probe for multiscale chiral structures, Proc. Natl. Acad. Sci. U.S.A. **118**, e2020055118 (2021).
[18] A. A. Sirenko, P. Marsik, C. Bernhard, T. N. Stanislavchuk, V. Kiryukhin, and S.-W. Cheong, Terahertz Vortex Beam as a Spectroscopic Probe of Magnetic Excitations, Phys. Rev. Lett. **122**, 237401 (2019).
[19] H. Fujita and M. Sato, Ultrafast generation of skyrmionic defects with vortex beams: Printing laser profiles on magnets, Phys. Rev. B **95**, 054421 (2017).
[20] H. Fujita and M. Sato, Encoding orbital angular momentum of light in magnets, Phys. Rev. B **96**, 060407(R) (2017).
[21] W. Yang, H. Yang, Y. Cao, and P. Yan, Photonic orbital angular momentum transfer and magnetic skyrmion rotation, Opt. Express **26**, 8778 (2018).
[22] G. Gariepy, J. Leach, K. T. Kim, T. J. Hammond, E. Frumker, R. W. Boyd, and P. B. Corkum, Creating High-Harmonic Beams with Controlled Orbital Angular Momentum, Phys. Rev. Lett. **113**, 153901 (2014).
[23] R. Géneaux, A. Camper, T. Auguste, O. Gobert, J. Caillat, R. Taïeb, and T. Ruchon, Synthesis and characterization of attosecond light vortices in the extreme ultraviolet, Nat. Commun. **7**, 12583 (2016).
[24] F. Kong, C. Zhang, F. Bouchard, Z. Li, G. G. Brown, D. H. Ko, T. J. Hammond, L. Arissian, R. W. Boyd, E. Karimi, and P. B. Corkum, Controlling the orbital angular momentum of high harmonic vortices, Nat. Commun. **8**, 14970 (2017).
[25] D. Gauthier, P. R. Ribič, G. Adhikary, A. Camper, C. Chappuis, R. Cucini, L. F. DiMauro, G. Dovillaire, F. Frassetto, R. Géneaux, P. Miotti, L. Poletto, B. Ressel, C. Spezzani, M. Stupar, T. Ruchon, and G. De Ninno, Tunable orbital angular momentum in high-harmonic generation, Nat. Commun. **8**, 14971 (2017).
[26] P. Rebernik Ribič, B. Rösner, D. Gauthier, E. Allaria, F. Döring, L. Foglia, L. Giannessi, N. Mahne, M. Manfredda, C. Masciovecchio, R. Mincigrucci, N. Mirian, E. Principi, E. Roussel, A. Simoncig, S. Spampinati, C. David, and G. De Ninno, Extreme-Ultraviolet Vortices from a Free-Electron Laser, Phys. Rev. X **7**, 031036 (2017).
[27] K. M. Dorney, L. Rego, N. J. Brooks, J. San Román, C.-T. Liao, J. L. Ellis, D. Zusin, C. Gentry, Q. L. Nguyen,

J. M. Shaw, A. Picón, L. Plaja, H. C. Kapteyn, M. M. Murnane, and C. Hernández-García, Controlling the polarization and vortex charge of attosecond high-harmonic beams via simultaneous spin–orbit momentum conservation, Nat. Photonics **13**, 123 (2019).

[28] L. Rego, K. M. Dorney, N. J. Brooks, Q. L. Nguyen, C.-T. Liao, J. S. Román, D. E. Couch, A. Liu, E. Pisanty, M. Lewenstein, L. Plaja, H. C. Kapteyn, M. M. Murnane, and C. Hernández-García, Generation of extreme-ultraviolet beams with time-varying orbital angular momentum, Science **364**, eaaw9486 (2019).

[29] E. Pisanty, L. Rego, J. San Román, A. Picón, K. M. Dorney, H. C. Kapteyn, M. M. Murnane, L. Plaja, M. Lewenstein, and C. Hernández-García, Conservation of Torus-Knot Angular Momentum in High-Order Harmonic Generation, Phys. Rev. Lett. **122**, 203201 (2019).

[30] E. Hemsing, A. Knyazik, M. Dunning, D. Xiang, A. Marinelli, C. Hast, and J. B. Rosenzweig, Coherent optical vortices from relativistic electron beams, Nat. Phys. **9**, 549 (2013).

[31] J. Vila-Comamala, A. Sakdinawat, and M. Guizar-Sicairos, Characterization of x-ray phase vortices by ptychographic coherent diffractive imaging, Opt. Lett. **39**, 5281 (2014).

[32] S. Sasaki, M. Hosaka, M. Katoh, T. Konomi, A. Miyamoto, and N. Yamamoto, Analyses of light's orbital angular momentum from helical undulator harmonics, in *6th International Particle Accelerator Conference (IPAC'15)* (JACoW, Geneva, Switzerland, 2015), p. TUPWA061, 10.18429/JACoW-IPAC2015-TUPWA061

[33] J. C. T. Lee, S. J. Alexander, S. D. Kevan, S. Roy, and B. J. McMorran, Laguerr-Gauss and Hermite-Gauss soft x-ray states generated using diffractive optics, Nat. Photonics **13**, 205 (2019).

[34] L. Loetgering, M. Baluktsian, K. Keskinbora, R. Horstmeyer, T. Wilhein, G. Schütz, K. S. E. Eikema, and S. Witte, Generation and characterization of focused helical x-ray beams, Sci. Adv. **6**, eaax8836 (2020).

[35] J. S. Woods, X. M. Chen, R. V. Chopdekar, B. Farmer, C. Mazzoli, R. Koch, A. S. Tremsin, W. Hu, A. Scholl, S. Kevan, S. Wilkins, W.-K. Kwok, L. E. De Long, S. Roy, and J. T. Hastings, Switchable X-Ray Orbital Angular Momentum from an Artificial Spin Ice, Phys. Rev. Lett. **126**, 117201 (2021).

[36] M. Fanciulli, D. Bresteau, M. Vimal, M. Luttmann, M. Sacchi, and T. Ruchon, Electromagnetic theory of helicoidal dichroism in reflection from magnetic structures, Phys. Rev. A **103**, 013501 (2021).

[37] X. Zhang, Y. Zhou, K. M. Song, T.-E. Park, J. Xia, M. Ezawa, X. Liu, W. Zhao, G. Zhao, and S. Woo, Skyrmion-electronics: Writing, deleting, reading and processing magnetic skyrmions toward spintronic applications, J. Phys. Condens. Matter **32**, 143001 (2020).

[38] A. Fernández-Pacheco, R. Streubel, O. Fruchart, R. Hertel, P. Fischer, and R. P. Cowburn, Three-dimensional nanomagnetism, Nat. Commun. **8**, 15756 (2017).

[39] T. Shinjo, Magnetic vortex core observation in circular dots of permalloy, Science **289**, 930 (2000).

[40] S. D. Bader, Colloquium: Opportunities in nanomagnetism, Rev. Mod. Phys. **78**, 1 (2006).

[41] M. Natali, I. L. Prejbeanu, A. Lebib, L. D. Buda, K. Ounadjela, and Y. Chen, Correlated Magnetic Vortex Chains in Mesoscopic Cobalt Dot Arrays, Phys. Rev. Lett. **88**, 157203 (2002).

[42] A magnetic vortex has the symmetry of a toroidal moment, in the sense defined by J. Hlinka [43]. The pointing direction of this toroidal moment is associated with the clockwise or counterclockwise curling direction (m) of the magnetic vortex. We use this denomination instead of the frequent but strictly speaking improper use of the term "chirality".

[43] J. Hlinka, Eight Types of Symmetrically Distinct Vectorlike Physical Quantities, Phys. Rev. Lett. **113**, 165502 (2014).

[44] H.-B. Braun, Topological effects in nanomagnetism: From superparamagnetism to chiral quantum solitons, Adv. Phys. **61**, 1 (2012).

[45] K. Y. Guslienko, X. F. Han, D. J. Keavney, R. Divan, and S. D. Bader, Magnetic Vortex Core Dynamics in Cylindrical Ferromagnetic Dots, Phys. Rev. Lett. **96**, 067205 (2006).

[46] F. Capotondi *et al.*, Invited article: Coherent imaging using seeded free-electron laser pulses with variable polarization: First results and research opportunities, Rev. Sci. Instrum. **84**, 051301 (2013).

[47] E. Allaria *et al.*, Highly coherent and stable pulses from the FERMI seeded free-electron laser in the extreme ultraviolet, Nat. Photonics, **6**, 699 (2012).

[48] See Supplemental Material at http://link.aps.org/supplemental/10.1103/PhysRevLett.128.077401 for further details on the experimental methods, data analysis procedure and numerical simulations.

[49] S. Fürhapter, A. Jesacher, S. Bernet, and M. Ritsch-Marte, Spiral interferometry, Opt. Lett. **30**, 1953 (2005).

[50] S. Valencia, A. Gaupp, W. Gudat, H.-C. Mertins, P. M. Oppeneer, D. Abramsohn, and C. M. Schneider, Faraday rotation spectra at shallow core levels: $3p$ edges of Fe, Co, and Ni, New J. Phys. **8**, 254 (2006).

[51] B. Rösner, F. Döring, P. R. Ribič, D. Gauthier, E. Principi, C. Masciovecchio, M. Zangrando, J. Vila-Comamala, G. De Ninno, and C. David, High resolution beam profiling of x-ray free electron laser radiation by polymer imprint development, Opt. Express **25**, 30686 (2017).

[52] M. J. Donahue and D. G. Porter, OOMMF User's Guide, Interagency Report NISTIR 6376, National Institute of Standards and Technology, Gaithersburg, 1999, 10.6028/NIST.IR.6376.

[53] P. Woźniak, I. D. Leon, K. Höflich, G. Leuchs, and P. Banzer, Interaction of light carrying orbital angular momentum with a chiral dipolar scatterer, Optica **6**, 961 (2019).

[54] J. Ni, S. Liu, G. Hu, Y. Hu, Z. Lao, J. Li, Q. Zhang, D. Wu, S. Dong, J. Chu, and C.-W. Qiu, Giant helical dichroism of single chiral nanostructures with photonic orbital angular momentum, ACS Nano **15**, 2893 (2021).

[55] M. T. Birch *et al.*, Real-space imaging of confined magnetic skyrmion tubes, Nat. Commun. **11**, 1726 (2020).

[56] W. Legrand, J.-Y. Chauleau, D. Maccariello, N. Reyren, S. Collin, K. Bouzehouane, N. Jaouen, V. Cros, and A. Fert, Hybrid chiral domain walls and skyrmions in magnetic multilayers, Sci. Adv. **4**, eaat0415 (2018).

[57] G. Spektor, D. Kilbane, A. K. Mahro, B. Frank, S. Ristok, L. Gal, P. Kahl, D. Podbiel, S. Mathias, H. Giessen *et al.*, Revealing the subfemtosecond dynamics of orbital angular

momentum in nanoplasmonic vortices, Science **355**, 1187 (2017).

[58] Y. Dai, Z. Zhou, A. Ghosh, R. S. K. Mong, A. Kubo, C.-B. Huang, and H. Petek, Plasmonic topological quasiparticle on the nanometre and femtosecond scales, Nature (London) **588**, 616 (2020).

[59] N. Kerber, D. Ksenzov, F. Freimuth, F. Capotondi, E. Pedersoli, I. Lopez-Quintas, B. Seng, J. Cramer, K. Litzius, D. Lacour, H. Zabel, Y. Mokrousov, M. Kläui, and C. Gutt, Faster chiral versus collinear magnetic order recovery after optical excitation revealed by femtosecond XUV scattering, Nat. Commun. **11**, 6304 (2020).

[60] F. Büttner *et al.*, Observation of fluctuation-mediated picosecond nucleation of a topological phase, Nat. Mater. **20**, 30 (2021).

[61] A. V. Kimel, A. Kirilyuk, P. A. Usachev, R. V. Pisarev, A. M. Balbashov, and T. Rasing, Ultrafast non-thermal control of magnetization by instantaneous photomagnetic pulses, Nature (London) **435**, 655 (2005).